DOT/FAA/AR-03/34

Office of Aviation Research
Washington, D.C. 20591

Comparison of Actual and Simulated Smoke for the Certification of Smoke Detectors in Aircraft Cargo Compartments

November 2003

Final Report

This document is available to the U.S. public through the National Technical Information Service (NTIS), Springfield, Virginia 22161.



U.S. Department of Transportation
Federal Aviation Administration

NOTICE

This document is disseminated under the sponsorship of the U.S. Department of Transportation in the interest of information exchange. The United States Government assumes no liability for the contents or use thereof. The United States Government does not endorse products or manufacturers. Trade or manufacturer's names appear herein solely because they are considered essential to the objective of this report. This document does not constitute FAA certification policy. Consult your local FAA aircraft certification office as to its use.

This report is available at the Federal Aviation Administration William J. Hughes Technical Center's Full-Text Technical Reports page: actlibrary.tc.faa.gov in Adobe Acrobat portable document format (PDF).

Technical Report Documentation Page

1. Report No.	2. Government Accession No.	3. Recipient's Catalog No.
DOT/FAA/AR-03/34		

4. Title and Subtitle	5. Report Date
COMPARISON OF ACTUAL AND SIMULATED SMOKE FOR THE CERTIFICATION OF SMOKE DETECTORS IN AIRCRAFT CARGO COMPARTMENTS	November 2003
	6. Performing Organization Code

7. Author(s)	8. Performing Organization Report No.
Jill Suo-Anttila, Walt Gill, and Louis Gritzo	

9. Performing Organization Name and Address	10. Work Unit No. (TRAIS)
Fire Science and Technology Sandia National Laboratories Fire Science and Technology Albuquerque, NM 87185-0836	11. Contract or Grant No.

12. Sponsoring Agency Name and Address	13. Type of Report and Period Covered
U.S. Department of Transportation Federal Aviation Administration Office of Aviation Research Washington, DC 20591	Final Report
	14. Sponsoring Agency Code ANM-110

15. Supplementary Notes

The FAA William J. Hughes Technical Center Technical Monitor was David Blake.

16. Abstract

Federal regulations require that aircraft cargo compartment smoke detection systems be certified by testing their operation in flight. For safety reasons, simulated smoke sources are permitted in these certification tests. To provide insight into smoke detector certification in cargo compartments, this research investigates the morphology, transport, and optical properties of actual and simulated smoke sources.

Experimental data show the morphology of the particulate in smoke from flaming fires is considerably different than simulated smoke. The particulate for all three different flaming fires was solid with similar morphological properties. Simulated smoke was composed of relatively large liquid droplets, and considerably different size droplets can be produced from a single simulated smoke machine. Transport behavior modeling showed that both actual and simulated smoke particulate are sufficiently small to follow the overall gas flow. However, actual smoke transport will be buoyancy-driven due to the increased temperature, while the simulated smoke temperature is typically low and the release may be momentum-driven. The morphology of the actual and simulated smoke were then used to calculate their optical properties. In contrast to the actual smoke, which is dominate by absorption, all the extinction for the simulated smoke is due to scattering. This difference could have an impact on detection criteria and, hence, time for photoelectric smoke detectors, since they alarm based on the scattering properties of the smoke.

17. Key Words	18. Distribution Statement
Smoke detection, Optical properties, Extinction, Scattering, Soot morphology, Simulated smoke, Smoke transport	This document is available to the public through the National Technical Information Service (NTIS) Springfield, Virginia 22161.

19. Security Classif. (of this report)	20. Security Classif. (of this page)	21. No. of Pages	22. Price
Unclassified	Unclassified	40	

ACKNOWLEDGEMENTS

Sandia is a multiprogram laboratory operated by Sandia Corporation, a Lockheed Martin Company, for the United States Department of Energy under contract DE-AC04-94AL85000. This work was performed in collaboration with the Federal Aviation Administration William J. Hughes Technical Center, Atlantic City International Airport, NJ, and NASA Glenn Research Center. The authors would like to acknowledge Dave Blake, Bob Filipczak, Louise Speitel, and other FAA Technical Center personnel for their assistance during the experiments when soot samples were obtained. The assistance of Mun Choi in the random analysis technique of measuring morphological properties is acknowledged. Reviews by David Glaze and Tom Lalk were also greatly appreciated.

TABLE OF CONTENTS

		Page
EXECUTIVE SUMMARY		ix
1.	INTRODUCTION	1
2.	EXPERIMENTAL APPROACH	1
2.1	Test Series	2
2.2	Fuel Sources	2
2.3	Experimental Facilities	4
2.4	Experimental Observations	5
2.5	Thermophoretic Sampling	6
2.5.1	Diagnostic Design	7
2.5.2	Transmission Electron Micrographs	8
2.6	Analysis of Morphology	8
2.6.1	Technique for Measuring Morphological Properties	8
2.6.2	Calculation of Fractal Properties	9
3.	MORPHOLOGICAL PROPERTIES	10
3.1	Actual Smoke Morphology	10
3.2	Uncertainty Analysis of Measurement Technique	14
3.3	Simulated Smoke Morphology	15
4.	TRANSPORT PROPERTIES	18
5.	OPTICAL PROPERTIES	20
5.1	Actual Smoke	21
5.2	Simulated Smoke	24
5.3	Application to Detection	26
6.	SUMMARY OF RESULTS AND CONCLUSION	27
6.1	Morphology	27
6.2	Transport	28
6.3	Optical Properties	29
6.4	Conclusion	30
7.	REFERENCES	30

LIST OF FIGURES

Figure		Page
1	Fuel Sources—Resin Cake, Jet A, and a Suitcase	2
2	Cone Calorimeter Facility	4
3	Intermediate-Scale Calorimeter Facility	5
4	Full-Scale B-707 Cargo Compartment Facility	5
5	Soot Collected on Filters—Smoldering and Flaming Resin	6
6	Transmission Electron Microscopy Image of Soot Aggregates	6
7	Grid Holder	7
8	Schematic Displaying Measured Soot Properties	9
9	Soot Aggregates (Resin, Jet A, and Suitcase)	10
10	Soot Morphology—Flaming Resin Cake	11
11	Soot Morphology—Suitcase	12
12	Soot Morphology—Jet A	13
13	Transmission Electron Microscopy Negative and Measurements of Polystyrene Spheres	15
14	Schematic of a Smoke Generator	16
15	Simulated Smoke Particle Size Distributions	17
16	Transport of Theatrical Smoke Droplets	19
17	Mass-Specific Extinction	23
18	Mass-Specific Scattering	23
19	Mass-Specific Absorption	23
20	Mass-Specific Coefficient for Simulated Smoke (0.3 micron)	25
21	Mass-Specific Coefficient for Simulated Smoke (0.66 micron)	25
22	Schematics of Smoke Detectors	26
23	Comparison of Scattering Properties	27

LIST OF TABLES

Table		Page
1	Smoke Characterization Experiments	3
2	Soot Morphology Results	13
3	Properties of Simulated Smoke Generators	16

LIST OF ACRONYMS AND SYMBOLS

N	Number of primaries
A_a	Agglomerate area (m^2)
A_p	Primary particle area (m^2)
d_p	Diameter of primary (m)
L	Aggregate length (m)
W	Aggregate width (m)
k_f	Fractal prefactor
D_f	Fractal dimension
R_g	Radius of gyration (m)
σ_{ext}	Mass specific extinction (m^2/g)
σ_{abs}	Mass specific absorption (m^2/g)
σ_{sca}	Mass specific scattering (m^2/g)
k_{ext}	Light extinction coefficient (1/m)
ρ	Density (kg/m^3)
λ	Wavelength (m)
M_s	Mass concentration (kg/m^3)
K_e	Dimensionless extinction coeffient
f_v	Volume fraction (m^3/m^3)
x_p	Size parameter
m	Complex index of refraction ($m=n-ik$)
$F(m)$	Function of the complex index of refraction
$E(m)$	Function of the complex index of refraction

CCD	Charge-coupled device
FAA	Federal Aviation Administration
RDG-PFA	Rayleigh-Debye-Gans theory for polydisperse fractal aggregates
TEM	Transmission Electron Microscopy

EXECUTIVE SUMMARY

Federal regulations require that smoke detection systems be certified by testing their operation in flight. For safety reasons, simulated smoke is often used for the required flight tests. It is, therefore, important to understand the similarities and differences of actual and simulated smoke. The purpose of this research was to characterize actual and simulated smoke sources to provide insight into the morphology, transport, and optical properties and to determine how the smokes would behave in smoke detector certification tests. In this study, a series of experiments were performed for the purpose of characterizing the morphology of actual smoke for fuel sources such as resin cakes, suitcases, and Jet A, which have been considered for use in certification tests. The transport properties of actual and simulated smoke were also compared using the results of the experiments and published simulated smoke data. Finally, with knowledge of the morphology and composition of actual and simulated smoke, the optical properties were calculated and compared.

In the experiments, a thermophoretic-sampling technique allowed for characterization of the flaming smoke since it contained the solid particulate required for imaging. The experiments allowed a quantitative characterization of actual smoke from flaming fires, while only a qualitative assessment of actual smoke from smoldering fires was feasible due to to the liquid nature of the collected sample. The smoke from flaming fires consisted of primary particles aggregated into wispy chains. The morphological properties of the solid particulate were consistent with those reported in the literature. Overall, the morphology of the smoke from the flaming fires of all three fuels was very similar, but when compared to simulated smoke, extreme differences were identified. Simulated smoke does not consist of solid particulate like actual smoke, and the individual droplets are considerably larger than the primary particles in actual smoke. In contrast to the relatively narrow distribution of actual smoke morphology, simulated smoke morphology can vary a great deal even for a single machine.

Based on the results of modeling transport behavior, it was determined that both actual and simulated smoke particulate are sufficiently small to follow the overall gas flow. It was observed that the transport may be different due to a difference in release temperatures and driving potential. Actual smoke transport will be buoyancy-driven due to the increased temperature, while the simulated smoke release temperature may be only very slightly elevated. In many cases, the simulated smoke could be forcefully expelled, which would make the transport momentum-driven instead of buoyancy-driven.

To calculate the optical properties, an appropriate theory was used based on the size parameter for the particulate. Rayleigh-Debye-Gans-polydisperse fractal aggregate theory was used for the three actual smokes, and it was found that scattering comprised up to 30% of the total extinction. Mie theory was used to calculate the optical properties of simulated smoke. In contrast to the actual smoke, all of the extinction for the simulated smoke was due to scattering. The extinction for the smaller droplets (0.3 micron) was approximately half of the total extinction for the actual smokes, while the extinction for the larger droplets was approximately the same as the actual smokes. The scattering for the smaller droplets was about the same as the actual smoke, but the scattering for the larger droplets was almost double the actual smoke scattering. This could have a great impact on detection time for photoelectric smoke detectors since they alarm based on the

scattering properties of the smoke. Calculation of the optical properties allows the smokes to be compared, and in addition, they can be used to calculate soot volume fraction from extinction measurements already being performed in the full-scale model validation experiments.

1. INTRODUCTION.

Federal regulations require that smoke detection systems be certified by testing their operation in flight. Flight tests typically use theatrical smoke generators to produce the necessary simulated smoke [1]. These simulated smoke generators are intended to be used in a manner representative of an actual fire scenario that could occur in a cargo compartment. Presently, a video of a burning suitcase is provided by the Federal Aviation Administration (FAA) William J. Hughes Technical Center, Atlantic City International Airport, NJ, to certifying officials so that a reasonable scenario can be selected and used in the certification tests. To supplement and improve the scenario selection, a computational fluid dynamics-based smoke transport model is being developed.

The purpose of this study was to provide a detailed comparison of the properties of actual and simulated smoke to determine if both smoke sources would interact with cargo compartment smoke detection systems in a similar manner. Smoke from combustion processes consists of both types of particulate matter, solid (commonly referred to as soot) and liquid, as well as gaseous products of combustion reactions. The smoke properties of importance can be categorized into two groups: properties used to characterize the source term in the transport model (mass flux, heat release, gaseous species concentrations, and soot volume fraction) and properties which affect smoke detection (composition, transport, and morphology). Experiments performed at the FAA Technical Center, using a cone calorimeter, an intermediate-scale calorimeter, and a full-scale cargo compartment test facility, allowed for the characterization of most of these properties for actual smoke. Since simulated smoke is commonly used in the detector certification process, characterization of its morphology, transport, and optical properties was also performed.

To meet the need of smoke characterization, detailed visual examination of the smoke particulate representative of a cargo compartment fire was performed as part of the ongoing experiments. Smoke samples were extracted both from fires in a full-scale cargo compartment and from calorimeter fire experiments. The collected samples were analyzed to develop a set of particulate morphology characteristics as a function of the fire type. Knowledge of soot morphology is useful in calculating soot volume fraction from extinction measurements in the full-scale model validation experiments. The morphology was also used to characterize transport and optical properties. Similarly, based upon knowledge of simulated smoke morphology, a characterization of the transport and optical properties was performed.

2. EXPERIMENTAL APPROACH.

Experiments were performed to characterize actual smoke at the FAA in the cone calorimeter, the intermediate-scale calorimeter, and the full-scale cargo compartment test facility. The cone calorimeter and intermediate-scale calorimeter experiments were performed to define a baseline fire and to characterize the fuel material in terms of the specific heat release rate, mass loss rate, product composition, and smoke obscuration. Fire experiments were conducted in a full-scale cargo test facility to gather data for formulating and validating the computational smoke transport model. Smoke particulate samples were collected during the execution of these tests. The sampling consisted of inserting a wand that supports a particle collection grid into the smoke flow for a predetermined period (on the order of seconds). The flame zone, or smoke region,

was easily accessible for the full-scale tests, and the grid holder was positioned by hand. For the calorimeter, the grid holder was inserted into the smoke exhaust pipe via a small hinged door provided by the FAA. At least three samples were taken at each condition to ensure that a sample suitable for image analysis was obtained.

2.1 TEST SERIES.

Experiments were conducted to determine the variation of smoke particulate features with the fire time/types (representing smoldering or flaming fires) and heat release rates (materials producing low or high maximum heat release rates). The test series, shown in table 1, includes detailed information about the test setup and progress. The designation, in the column labeled FAA, indicates where the experiment was performed. The type of fire, flaming or smoldering, is listed in the fire source column. The subsequent columns describe the fuel, the ignition source, and the experimental observations.

2.2 FUEL SOURCES.

Three fuel sources, shown in figure 1, were studied in the test series: resin cakes, Jet A, and suitcases. The suitcases represent the most realistic fuel source, but smoke transport analysis is not as feasible since they do not burn repeatably. All suitcases were packed identically with cotton rags and were ignited by passing an electric current throught a nichrome wire within the suitcase. The suitcases initially smoldered and then transitioned to flaming as the experiment progressed.



FIGURE 1. FUEL SOURCES—RESIN CAKE, JET A, AND A SUITCASE

The resin cakes were designed and manufactured by the FAA Technical Center and were formulated to provide a repeatable fire source to be used in smoke transport experiments. Pressed pellets (PVC, PE, PS, Nylon, PBT, and PU) of known quantity comprise the resin cakes. A nichrome wire with a controlled length and spatial distribution is embedded within the resin cakes, which is capable of providing smoldering fires. Flaming fires are produced by running an electric current through the nichrome and by igniting a small amount of heptane placed on the resin cake.

TABLE 1. SMOKE CHARACTERIZATION EXPERIMENTS

Test	FAA	Fire Source	Fuel	Ignition Source	Notes
1	B707	Smoldering	3/8″ Resin Cake	360 W embedded 1/8″	Short soot sample at 45 sec
2	B707	Smoldering	3/8″ Resin Cake	360 W embedded 1/8″	Medium soot sample at 60 sec
3	B707	Smoldering	3/8″ Resin Cake	360 W embedded 1/8″	Long soot sample at 45 sec, extra long sample at 60 sec
4	B707	Flaming	3/8″ Resin Cake/Heptane (2 ml)	360 W embedded 1/8″ 10000V Continuous Spark 3/32″ Gap within 1/8″ of surface	Short soot sample at 45 sec
5	B707	Flaming	3/8″ Resin Cake/Heptane (2 ml)	360 W embedded 1/8″ 10000V Continuous Spark 3/32″ Gap within 1/8″ of surface	Medium soot sample at 60 sec
6	B707	Flaming	3/8″ Resin Cake/Heptane (2 ml)	360 W embedded 1/8″ 10000V Continuous Spark 3/32″ Gap within 1/8″ of surface	Long soot sample at 45 sec, extra short sample at 60 sec
7	Cone Calorimeter	Smoldering	3/8″ Resin Cake	360 W embedded 1/8″	60-sec baseline power applied at 60 sec, smoldered until 240 sec, short soot sample 45 sec after power applied
8	Cone Calorimeter	Smoldering	3/8″ Resin Cake	360 W embedded 1/8″	60-sec baseline power applied at 60 sec, smoldered until 240 sec, medium soot sample 60 sec after power applied
9	Cone Calorimeter	Smoldering	3/8″ Resin Cake	360 W embedded 1/8″	60-sec baseline power applied at 60 sec, smoldered until 173 sec transitioned to flaming. Power to wire shutoff for 5 sec and then restored until 240 sec, long soot sample 45 sec, extra long sample at 60 sec after power applied
10	Cone Calorimeter	Flaming	3/8″ Resin Cake/Heptane (2 ml)	360 W embedded 1/8″ 10000V Continuous Spark 3/32″ Gap within 1/8″ of surface	60-sec baseline power applied at 60 sec, started flaming until 240 sec, short soot sample 45 sec after power applied
11	Cone Calorimeter	Flaming	3/8″ Resin Cake/Heptane (2 ml)	360 W embedded 1/8″ 10000V Continuous Spark 3/32″ Gap within 1/8″ of surface	60-sec baseline power applied at 60 sec, started flaming until 240 sec, medium soot sample 60 sec after power applied
12	Cone Calorimeter	Flaming	3/8″ Resin Cake/Heptane (2 ml)	360 W embedded 1/8″ 10000V Continuous Spark 3/32″ Gap within 1/8″ of surface	60-sec baseline power applied at 60 sec, started flaming until 240 sec, short soot sample 45 sec, extra short 60 sec after power applied
13	B707	Smoldering	Suitcase	5 paper towels wrapped with 8 ft nichrome - 1 ohm/ft 65V	Short sample during smoldering at 30 seconds after power applied. Torch applied at 110 seconds
14	Intermediate - scale Calorimeter	Smoldering	Suitcase	5 paper towels wrapped with 8 ft nichrome - 1 ohm/ft 65V	60-sec baseline power applied at 60 sec, started smolder until 210 sec, short soot sample 105 sec after power applied
15	B707	Flaming	Suitcase	Continuation of test 13 with Butane ignitor	Short sample during flaming at 220 seconds after power applied. Torch applied at 110 seconds
16	Intermediate - scale Calorimeter	Flaming	Suitcase	Continuation of test 14 self-ignited	60-sec baseline power applied at 60 sec, started smolder until 210 sec, self- ignited and burned until end of test. Short sample at 30 sec after ignition.
17	Cone Calorimeter	Flaming	Jet A (15 ml)/ Heptane (4 ml) 3.5″ Dia	Butane Ignitor	60-sec baseline torch applied at 60 sec, started flaming until 240 sec, short soot sample 20 sec after ignition, short sample 110 sec after ignition
18	B707	Flaming	Jet A (15 ml)/ Heptane (4 ml) 5.0″ Dia	10000V Continuous Spark 3/32″ Gap within 1/4″ of surface	3 minutes total burn time, short sample at 45 sec after ignition, medium sample at 60 secs after ignition

Liquid Jet A fuel was also used in the experiments. These small flaming pan fires were initially used as the repeatable fire source before the resin cakes were developed. The resin cakes were deemed more suitable since they were comprised of fuels commonly found in luggage and could

sustain either flaming or smoldering fires. Soot characterization was performed on the jet fuel for comparison with flaming resin cakes and previous large-scale JP-8 jet fuel experiments [2]. Using these three sources allowed comparison of the actual fuel source (i.e., suitcase) to repeatable fuel sources (resin cakes and Jet A) designed to simulate the actual source characteristics.

2.3 EXPERIMENTAL FACILITIES.

Two calorimeters were used to provide detailed information during the fires (i.e., heat release, species, etc.). The cone calorimeter was used to perform smoldering and flaming tests using resin cakes and Jet A as fuels. The cone calorimeter facility, shown in figure 2, is a standard American Society for Testing and Materials device. Typically, a sample is placed on a fixture and heated from above with a radiant heat lamp. For the resin cake, the radiant heat lamp was replaced with power input by the nichrome wire imbedded in the sample. During the test, the decomposition products are captured and analyzed, while the sample is continuously weighed to determine a mass loss. The intermediate-scale calorimeter, shown in figure 3, was used for the smoldering/flaming suitcase experiment. In this setup, an enclosed cabinet is used to contain and capture the products of decomposition. The products are then routed to the cone calorimeter sampling section for analysis. Soot samples were obtained from the calorimeter fires via a small hinged door in the sample section. The full-scale experiments were performed in an actual B-707 cargo compartment using all three fuel sources (see figure 4).

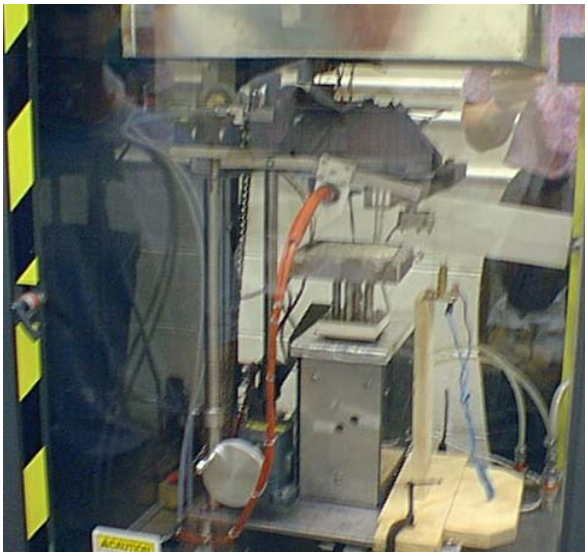

FIGURE 2. CONE CALORIMETER FACILITY



FIGURE 3. INTERMEDIATE-SCALE CALORIMETER FACILITY

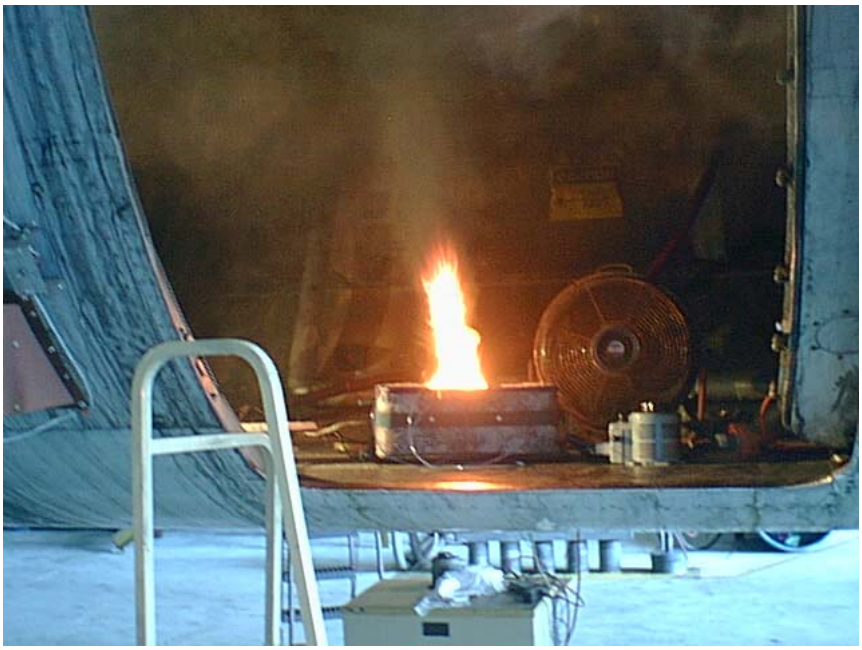

FIGURE 4. FULL-SCALE B-707 CARGO COMPARTMENT FACILITY

2.4 EXPERIMENTAL OBSERVATIONS.

The data collected in these experiments include fuel mass loss rate, species production rate, heat release rate, and smoke obscuration [3]. The focus of this study is on the smoke properties, in particular, the morphology that affect detection.

A notable difference in the smoldering and flaming fires was the appearance of the smoke. Smoldering fires produced white smoke, while flaming fire smoke appeared darker. The difference in color of the smoke was also evident upon visual inspection of the filter installed in the cone sampling section. The smoldering fire soot was yellow in color, while the flaming fire soot was black, as shown in figure 5.

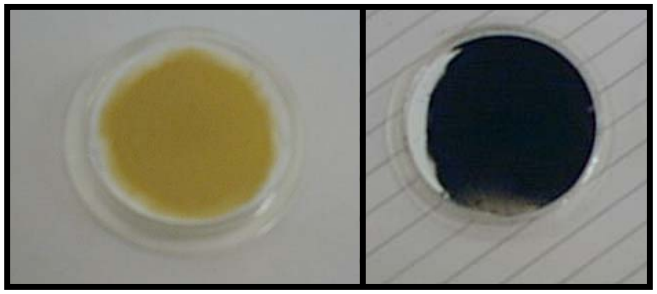

FIGURE 5. SOOT COLLECTED ON FILTERS—SMOLDERING AND FLAMING RESIN

2.5 THERMOPHORETIC SAMPLING.

The particulate matter (i.e., soot) present in smoke from burning materials or fuels can be characterized by transmission electron microscopy (TEM) imaging of samples obtained from the fires. To obtain a sample, a TEM grid is briefly inserted into the fire to collect soot particles. The particles in the flow are drawn to the grid due to thermophoresis (the attraction produced by the temperature gradient between the flow gas and the grid) and impingement of the flow on the grid. The grid is then taken to the transmission electron microscope where the soot particles are imaged. Figure 6 shows a JP-8 fuel fire TEM image, which displays aggregated soot primary particles. The diagnostic design and sample collection are described in the sections that follow.

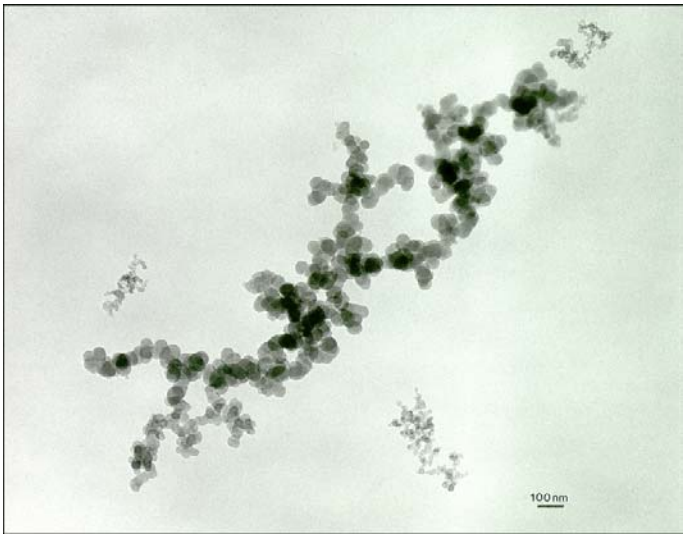

FIGURE 6. TRANSMISSION ELECTRON MICROSCOPY IMAGE OF SOOT AGGREGATES

2.5.1 Diagnostic Design.

A grid holder was designed specifically for the experiments in the FAA calorimeters and the full-scale B-707 cargo compartment. The design is based on previous experience in large jet fuel pool fires [2]. This new grid holder is much smaller than the one used in large fire experiments to minimize the impact on the flow field. A schematic and photograph of the grid holder are shown in figure 7.

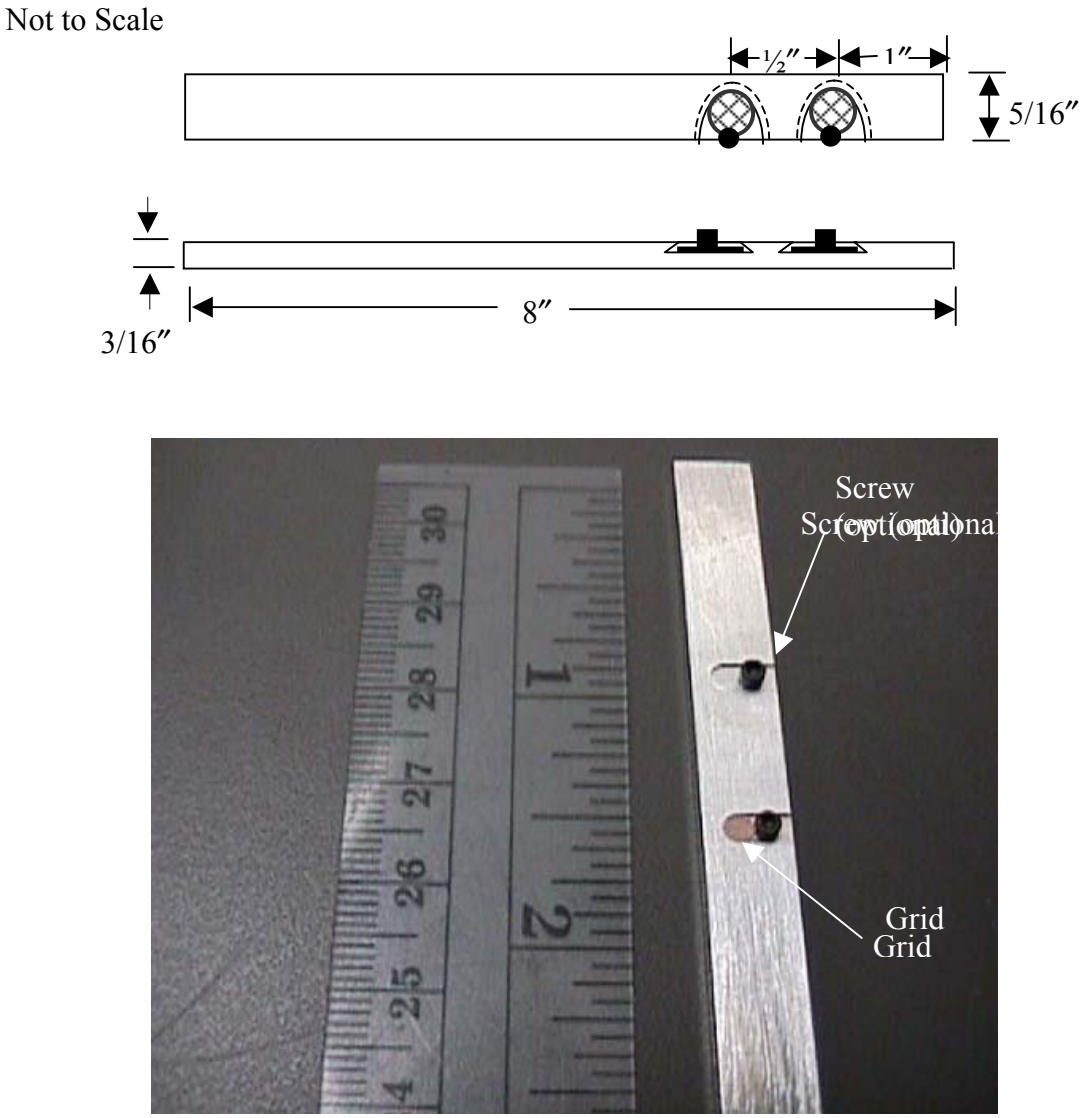

FIGURE 7. GRID HOLDER

The grids are held in a small slot in an aluminum bar. An optional set-screw is shown holding the grids in place. The grid holder was inserted into the flow and oriented such that the soot impinges directly on the grids. The flame zone, or smoke region, was easily accessible in the full-scale tests and the grid holder was positioned into the soot region. For the calorimeter experiments, the grid holder was inserted into the smoke exhaust pipe via a small hinged door.

Several different exposure times were used for each test case to ensure that a suitable sample was obtained.

2.5.2 Transmission Electron Micrographs.

Samples obtained from the test series, shown in table 1, were imaged with a TEM. Several samples were obtained for each test type, and the sample with the best soot coverage was chosen for analysis. Overall, the soot samples obtained from the flaming fuel fires produced good soot coverage for exposure times of approximately 1 second.

It was not possible to image the soot from any of the smoldering fires. The grids appeared almost clean except for a possible coating on the grid. A residue was slightly visible on the grid, but it was not possible to analyze its composition. Although the smoldering samples were not suitable for analysis, five samples from flaming fires were imaged. The imaged samples included:

- Flaming resin in the B-707 cargo compartment (test 4)
- Flaming resin in the cone calorimeter (test 10)
- Flaming suitcase in the B-707 cargo compartment (test 15)
- Flaming suitcase in the intermediate-scale calorimeter (test 16)
- Flaming pan of Jet A in the B-707 (test 18)

2.6 ANALYSIS OF MORPHOLOGY.

All soot samples obtained were imaged using a TEM. Approximately 20 micrographs, similar to figure 6, were obtained for each sample. The imaged areas for the micrographs were randomly selected from the entire grid area. A complete analysis, as described in the sections that follow, was performed using the images to gain a statistically significant characterization of the soot morphology of the sample.

2.6.1 Technique for Measuring Morphological Properties.

To convert the micrograph into an image suitable for analysis, it was placed on a light table and imaged via a high-resolution, charge-coupled device (CCD) camera. The image captured by the CCD camera was digitized prior to analysis. The CCD camera is also capable of magnifying the image for detailed measurements. The contrast between the soot particles and the background was digitally enhanced to allow some measurements to be automated. Soot properties of interest included the dimension and area of primary particles and aggregates, since they influence the optical properties needed for sensing the smoke. The soot primary particle size (D_p) was obtained by manually measuring the diameter of soot particles within the aggregates. Other measurements included the projected area of the primary particles (A_p) and the projected area of the aggregate (A_a), as shown in figure 8.

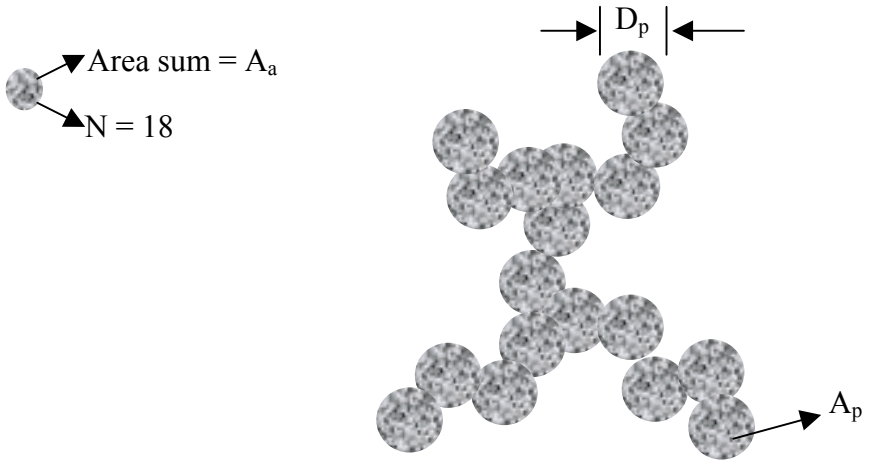

FIGURE 8. SCHEMATIC DISPLAYING MEASURED SOOT PROPERTIES

2.6.2 Calculation of Fractal Properties.

Since soot can be considered a fractal aggregate, the extinction coefficient (σ_{ext}) is based on the number of primaries in an aggregate (N), the fractal dimension (D_f), and the fractal prefactor (k_f). These quantities, typically used to characterize soot morphology, can be extracted from the measured quantities in the following manner.

The number of primary particles comprising an aggregate is calculated using an empirical correlation [4]

$$N = \left[\frac{A_a}{A_p} \right]^{1.09} \tag{1}$$

where A_a and A_p are the projected areas of the agglomerate and primary particle, respectively, and N is the total number of particles comprising the aggregate. Soot aggregate structure is too sparse for it to be described as a compact sphere, and thus, the mass fractal analysis provides a useful relationship to determine the radius of gyration (R_g) based on primary particle size and the number of primary particles comprising the aggregate:

$$R_g = \sqrt{\frac{1}{N} \sum_{i=1}^{N} (r_i - r_c)^2} \tag{2}$$

where r_i is the centroid of the primary particle, and r_c is the centroid of the agglomerate. Since it is difficult to identify each individual particle that constitutes an aggregate, the R_g calculation formulation was revised by considering each pixel to be the individual element of interest. This approximation is valid since the average contribution to the total R_g from the subelements (pixels) that constitute the primary particle is equal to the contribution from a primary particle to

the total R_g. The equation for the radius of gyration remains the same, but N (determined by performing a histogram distribution of all pixels with graylevel greater than the threshold) now corresponds to the total number of pixel elements comprising the agglomerate (typically on the order of 20-30 thousand pixels).

Finally, the fractal prefactor (k_f) and the fractal dimension (D_f) can be determined based on either of the following equations [3 and 4]. A ln-ln plot reveals D_f and k_f.

$$N = k_f \left[\frac{R_g}{d_p} \right]^{D_f} \tag{3}$$

$$N = k_f \left(\frac{(LW)^{\frac{1}{2}}}{d_p} \right)^{D_f} \tag{4}$$

3. MORPHOLOGICAL PROPERTIES.

3.1 ACTUAL SMOKE MORPHOLOGY.

Thermophoretic sampling successfully allowed the characterization of soot morphology for all three fuels—resin cake, Jet A, and suitcase (see figure 9). Samples for the resin and suitcase fuels were obtained in both calorimeters and the full-scale B-707 cargo compartment. The Jet A sample was captured in the B-707 cargo compartment.

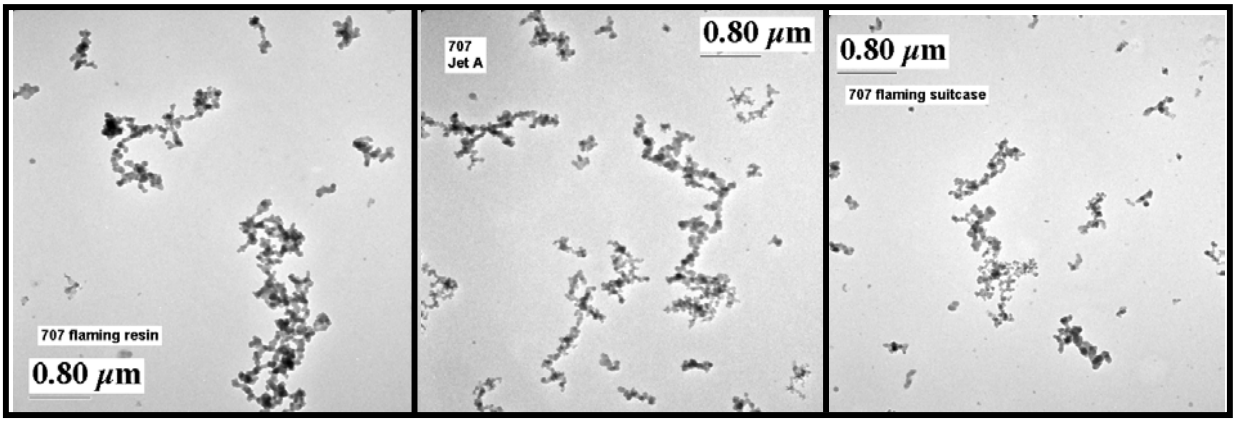

FIGURE 9. SOOT AGGREGATES (RESIN, JET A, AND SUITCASE)

The samples were characterized using the technique described in section 2. The results are displayed in figures 10 through 12 and are summarized in table 2. Samples were also obtained from fires within the cone calorimeter, but only the results from the full-scale B-707 test facility are displayed in the table. The results from the calorimeter did not differ from the B-707 results by more than 7%, and in most cases, the difference was only 3%.

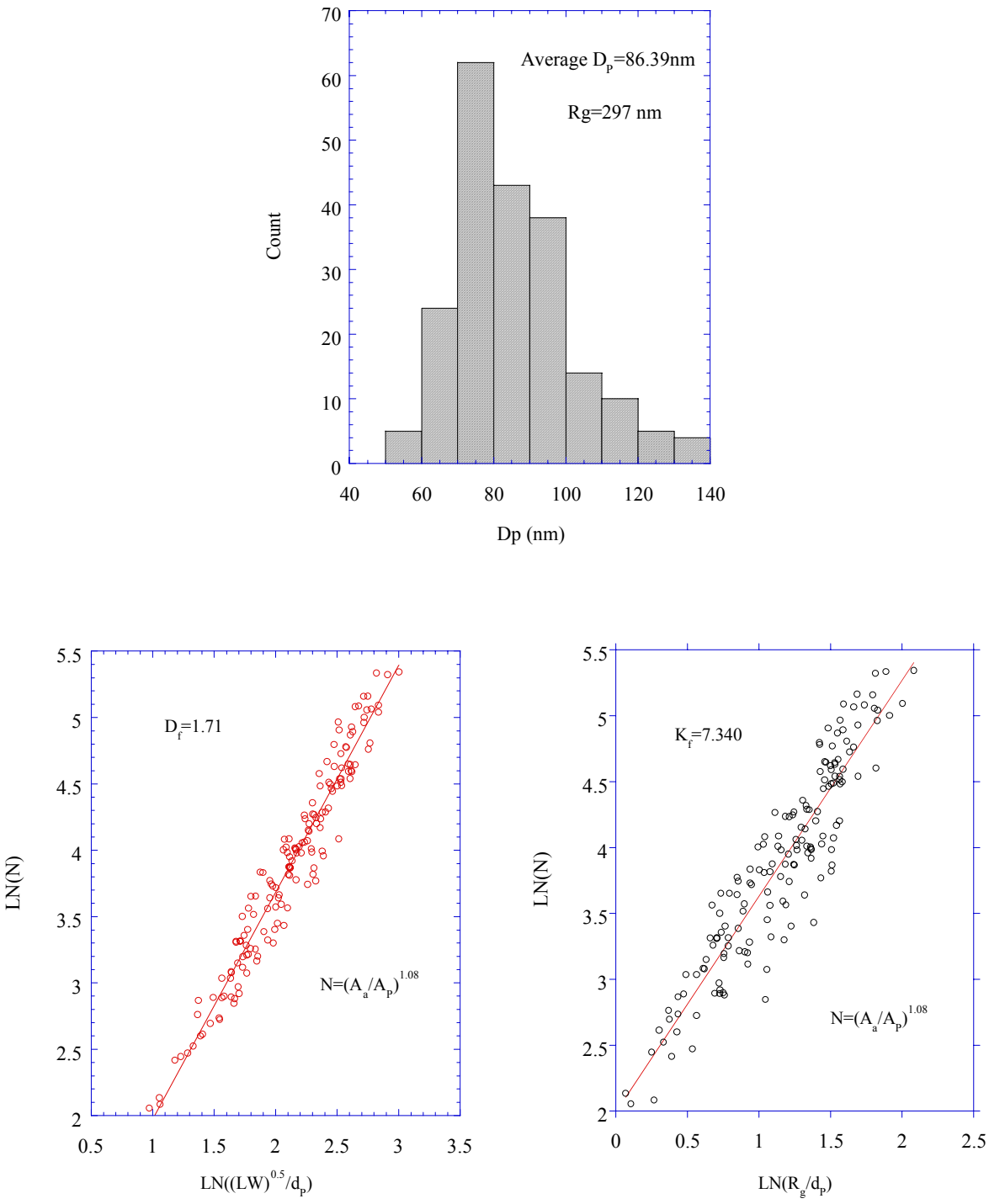

FIGURE 10. SOOT MORPHOLOGY—FLAMING RESIN CAKE

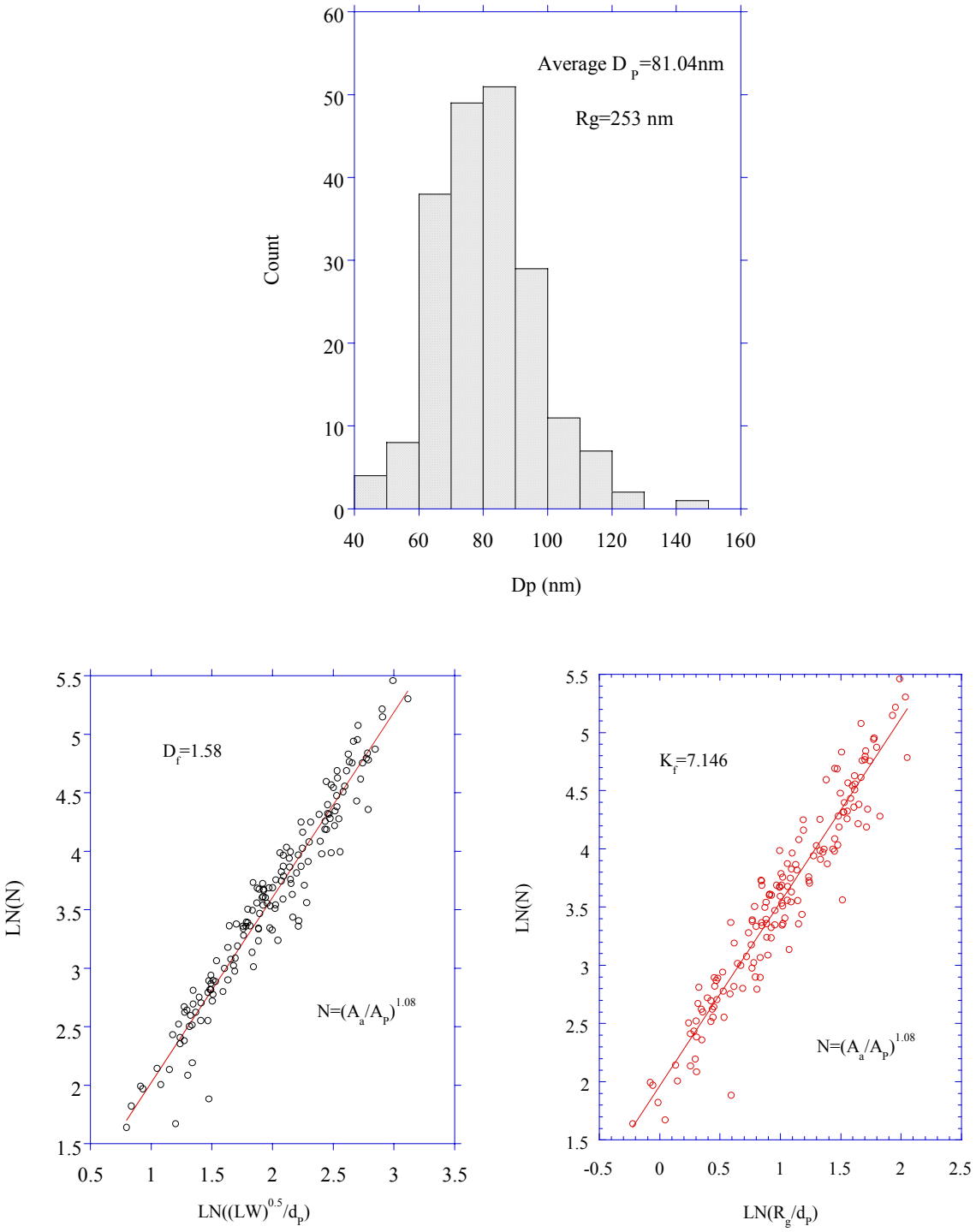

FIGURE 11. SOOT MORPHOLOGY—SUITCASE

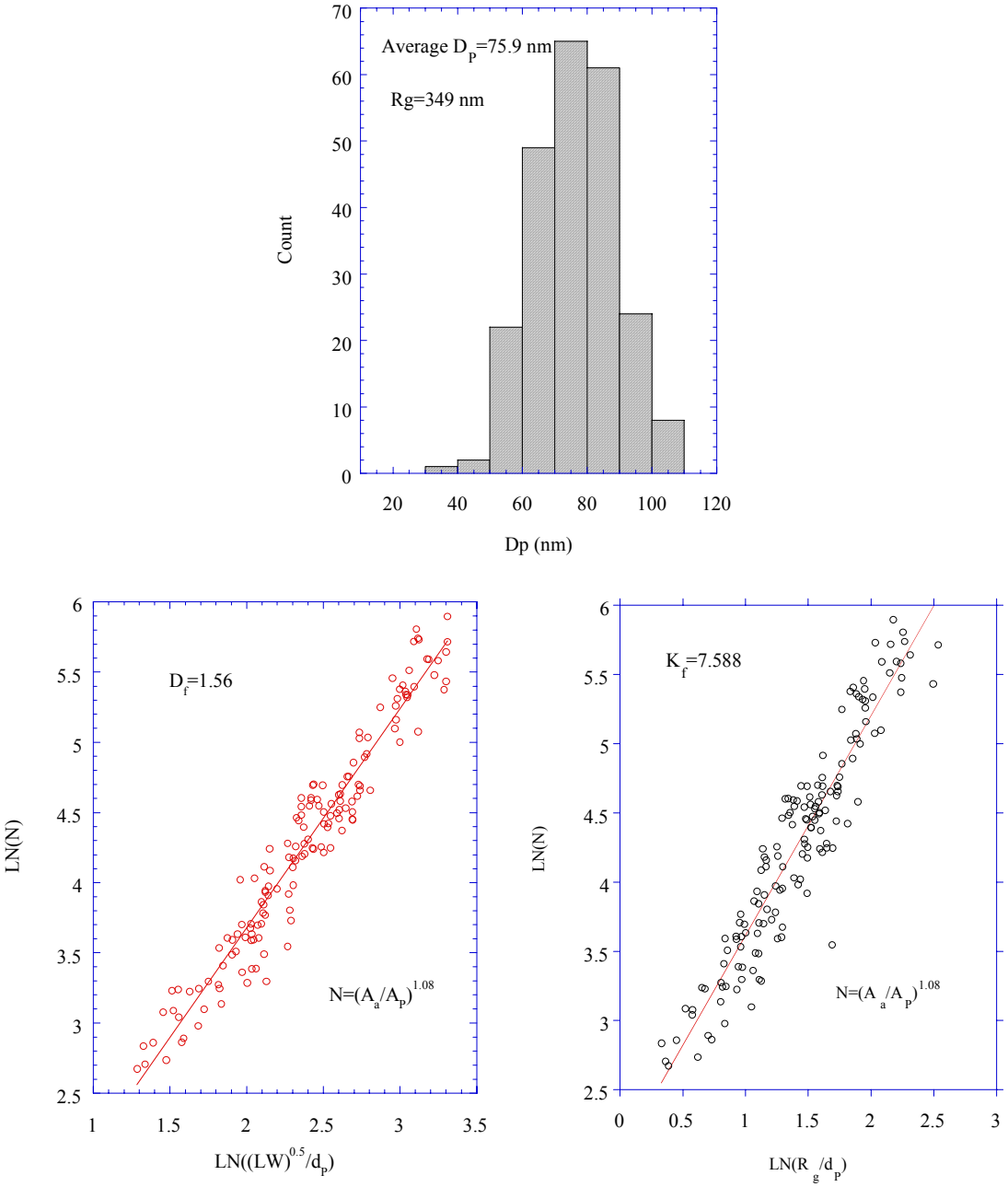

FIGURE 12. SOOT MORPHOLOGY—JET A

TABLE 2. SOOT MORPHOLOGY RESULTS

	D_p	k_f	D_f	R_g
Resin B-707	86.4 nm	7.34	1.71	297 nm
Suitcase B-707	81.0 nm	7.15	1.58	253 nm
Jet A B-707	75.9 nm	7.59	1.56	349 nm

The first parameter used to describe the morphology is the diameter of the primary particles (D_p). In all fuel samples there was a range of primary particles collected, typically between 40 and 140 nm. The average primary particle size from all fuels was approximately 80 nm. These primary particles aggregated into wispy chains up to several microns in length, as shown in figure 9.

The radius of gyration was obtained directly from the image (as in section 2) and gives an indication of the size of the agglomerate (average distance from the centoid to the edge of the agglomerate). The radius of gyrations calculated ranged from 253-349 nm. Also calculated directly from the images was the number of primary particles (N) per agglomerate.

Since soot is a fractal aggregate, the measured quantities (D_p, R_g, and N) can be used to compute the fractal dimension (D_f) and the fractal prefactor (k_f) based on the fractal power law for aggregates (shown in equation 3). The fractal prefactors calculated for the different fuels were very similar, ranging from 7.15 to 7.59. The fractal dimensions were also very similar (1.56-1.71). The fractal dimension gives an indication of the compactness of the aggregate. For reference, a straight line has a fractal dimension of 1, a two-dimensional plane has a fractal dimension of 2, and a sphere has a fractal dimension of 3. The average fractal dimension of approximately 1.6 is consistent with the TEM images and is commonly described as a wispy chain.

Overall, the morphology of the soots studied is consistent with a variety of soots documented in the literature [4, 5, and 6]. The soot consists of spherical primary particles aggregated into a wispy chain of fractal dimension less than 2. The average primary particle size is approximately 80 nm for all samples. Although the fractal dimension and fractal prefactor measured are similar to literature values, the measured average size of the primaries is larger than is typically stated in the literature [4, 5, and 6]. A thorough investigation of the measurement technique was performed, including quantitative characterization of the accuracy and uncertainty of the process. In general, the soots studied here are very similar in their morphological characteristics, and substitution of one source for another (i.e., resin cake instead of a suitcase) should not cause a significant difference in the morphology of the soot used in a particular experiment.

3.2 UNCERTAINTY ANALYSIS OF MEASUREMENT TECHNIQUE.

An estimate of the uncertainty in the measurement technique was performed by creating TEM micrographs of polystyrene spheres. Three different sized polystyrene spheres were mixed and deposited on a grid. The grid was then imaged to produce a negative in exactly the same way the soot grids were imaged and analyzed. The individuals performing the analysis of the grid were not informed of the size of the spheres deposited on the grid.

When analyzing soot images, the random analysis technique takes only a sampling of the total number of primary particles to represent the overall average. For the polystyrene sphere analysis, an estimate of the error in this sampling was sought by increasing the sample number until all spheres were imaged. In addition, the measurement of all spheres in the captured image provided an estimate of the accuracy of the automatic measurement technique. If the measurements were accurately performed, a multimodal distribution would be seen. The peaks would correspond to the size of the spheres stated by the manufacturer.

The diameter of the polystyrene spheres were 79, 93, and 173 nm. A sample image is shown in figure 13. The figure was scanned directly from the negative. In the analysis of the TEM micrographs, 12 regions were identified and then the spheres were measured in the regions. To obtain a particle size distribution for the overall population, all the spheres (668 total) within the selected regions were measured. Then a representative sample was obtained by only measuring random spheres (121 total) within the regions. This allowed assessment of the random technique as well as the accuracy of the measurement technique. It was concluded that the random technique allowed for characterization of the sphere diameters within an average of 8%. The histograms obtained are also shown in figure 13. A very similar distribution is shown in both the total population and the random sampling, and the peaks are in line with the sphere sizes, showing that the calibration and measurements are being correctly performed. Overall, confidence in the technique was obtained.

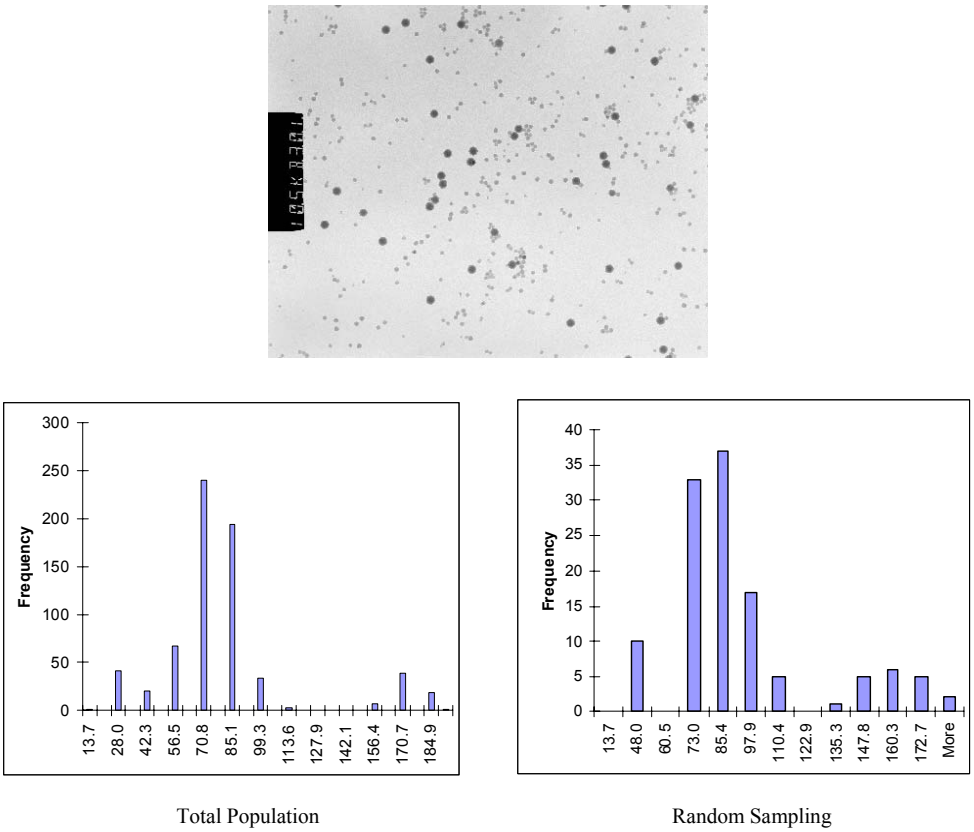

Total Population

Random Sampling

FIGURE 13. TRANSMISSION ELECTRON MICROSCOPY NEGATIVE AND MEASUREMENTS OF POLYSTYRENE SPHERES

3.3 SIMULATED SMOKE MORPHOLOGY.

Simulated smoke is produced by heating a liquid above its vaporization temperature. The vaporized liquid is then expelled from the heating chamber into the environment where it condenses, forming a fog-like smoke. Simulated smoke could not be characterized via thermophoretic sampling, like the three fuels described in section 2.2, due to the liquid nature of

the simulated smoke. As mentioned previously, imaging via TEM requires solid, opaque particles or objects.

Since simulated smoke could not be characterized using thermophoretic sampling, the properties of the simulated smoke were obtained from the manufacturer. Some of the data obtained from various manufacturers of simulated smoke machines are shown in table 3.

TABLE 3. PROPERTIES OF SIMULATED SMOKE GENERATORS

Supplier	Composition	Driving Potential	Temperature	Mass Flux (cfm)	Diameter (microns)
1	glycol/oil	Vapor press (CO_2)		3400 max	0.2-0.3
2	glycol	Vapor press (pump)	380°-480°F	20,000 max	?
3	glycol	Vapor press (pump)	80°-100°F	2,500-35,000 fixed	?
4	secret	Vapor press (pump)	212°-470°F	variable	0.25-60 (4avg)
5	glycol & glycerols	3-4 m plume	60°C nozzle	?	0.5
6	Proprietary fluid			5000 max	0.5-0.7

Upon request, more detailed data was obtained from a manufacturer (#1) who stated that their smoke generators are used in certification of aircraft smoke detectors, although the validity of this claim has not been investigated. A schematic of a smoke generator is shown in figure 14.

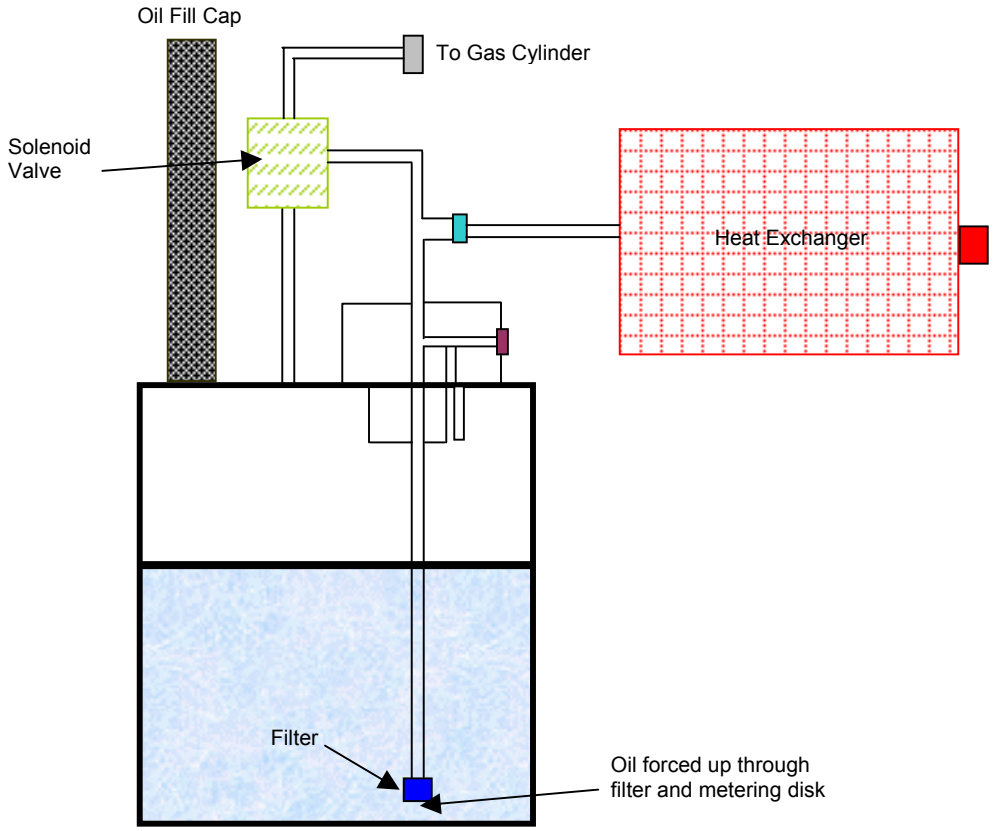

FIGURE 14. SCHEMATIC OF A SMOKE GENERATOR

The manufacturer states that running for 10 minutes at the maximum output, the smoke generator will consume 0.62 kg of oil fluid and 0.5 kg of CO_2 for driving potential. The fog produced by the simulated smoke generator consists of oil droplets that have recondensed upon exiting the heat exchanger. Measurement of the droplets was performed based on the scattered intensity of laser light to allow for a quantitative comparison between different machine settings and actual smoke from a combustion process. The particle size distribution was obtained for various machine settings (see figure 15). The different settings were referred to as

- 100 psi, standard setting (with nozzle at 314°C)
- 100 psi thin, dry setting
- 100 psi ultrathin setting
- Very wet setting

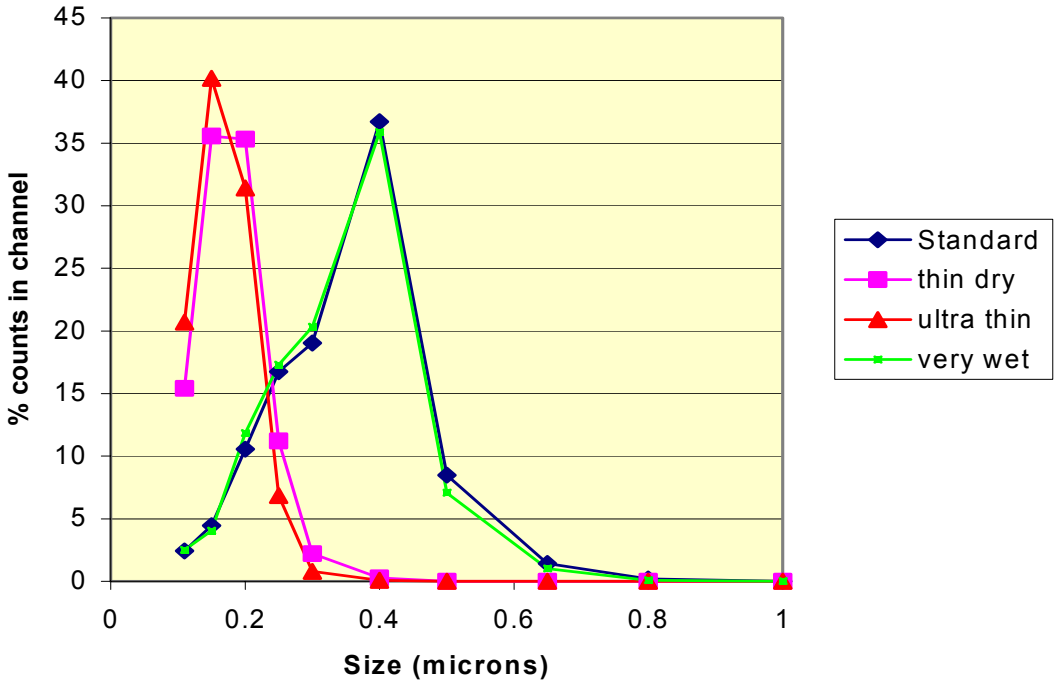

FIGURE 15. SIMULATED SMOKE PARTICLE SIZE DISTRIBUTIONS

The count and mass mean diameter for both the thin dry and the ultrathin settings was 0.15 and 0.17 micron, respectively. The standard and very wet count mean was 0.29 micron, while the mass mean was approximately 0.36 micron. The factor of 2 difference in the average size could greatly impact detection times, therefore, the setting should be consistent when certifying aircraft smoke detectors. It should also be noted that the size of the simulated smoke droplets is considerably larger than the actual smoke primary particles. In the case of the generator tested, the droplets are 2-3.5 times larger than actual smoke, but another smoke generation machine (listed as being acceptable for smoke detection tests [1]) reports considerably larger droplets (up to 60 microns which is 750 times larger than the primary particle size of actual smoke). The spectrum of different simulated smoke will result in different transport properties and detection times.

4. TRANSPORT PROPERTIES.

Knowledge of the morphology of real and simulated smoke allows an assessment of the transport properties of the smoke to be made. It is typically assumed that soot particles are small enough to follow the overall gaseous flow, allowing the soot particulates to be transported with the buoyant plume to upper regions of the cargo bay. These regions can potentially contain smoke detectors; therefore, detection times are dependent on transport of smoke containing particles or droplets to the area. If the particulates are large enough that they do not follow the flow, a fall-out of particles from the plume could impact detection times. Since theatrical smoke droplets can be considerably larger than soot particles, a calculation was performed to determine when the droplets would no longer follow the flow.

The analysis of the transport properties of simulated smoke was performed by writing a short computer code capable of calculating the forces on the droplet for varying droplet size, droplet properties, and velocity. The two forces existing are the drag force and the weight defined as

$$F_{weight} = \rho_{drop} g \left\{ \frac{4}{3} \pi \left(\frac{D_{drop}}{2} \right)^3 \right\} \tag{5}$$

$$F_{drag} = 0.5 \rho_{air} \left(\frac{V_{air}^{\ 2}}{2} \right) \pi \left(\frac{D_{drop}}{2} \right)^2 C_D \tag{6}$$

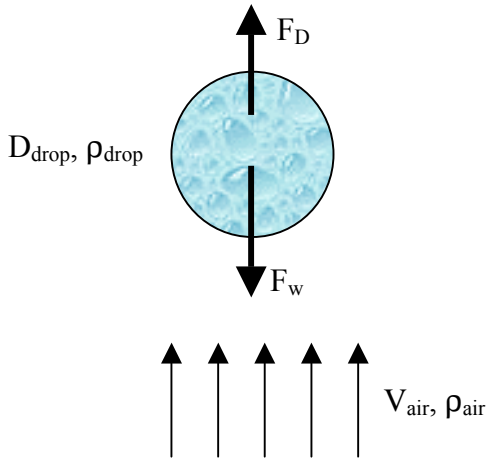

where C_D is based upon correlations for a sphere that depends on the magnitude of the Reynolds number (*Re*).

The net force was calculated for various droplet sizes and velocities. Two commonly used theatrical smoke droplet compositions (paraffin and a proprietary fluid) were analyzed. The two types of droplets differed in density. Paraffin density is 900 kg/m^3, while the proprietary fluid is 1100 kg/m^3. The results from the analysis are presented in figure 16. The vertical axis shows the air velocity that must be present to counteract the weight of the droplet. This velocity could also be considered the settling velocity of the droplet. For air velocities lower than this value, the force due to the weight will be greater than the drag force, thus the particle will not follow the flow. Since the proprietary fluid has a greater density, the force due to the weight is also greater and a larger air velocity is required for the particle to be transported with the flow. The average diameter for the proprietary droplet is approximately 4 microns, while the paraffin smoke generator, being considered for use by the FAA, is approximately 0.66 micron. In either case, the droplet could be considered small enough to be transported with the flow since the force on the particle due to the weight is significantly smaller than the drag force on the particle

due to the flow. Soot primary particles are typically less than 0.08 micron and, even when agglomerated into sparsely packed chains up to several microns in length, will follow the flow.

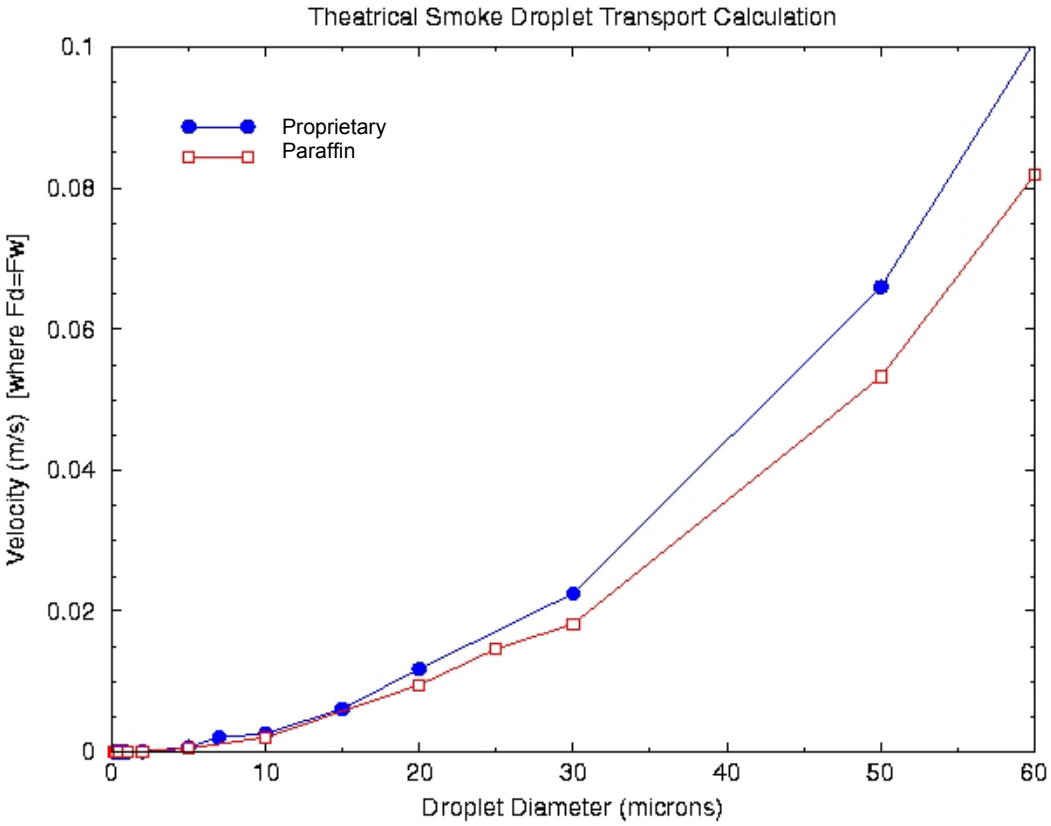

FIGURE 16. TRANSPORT OF THEATRICAL SMOKE DROPLETS

Although it has been shown that simulated smoke droplets are small enough to follow the flow, the transport of simulated smoke may be quite different from actual smoke, due in part to the potentially different release temperatures. Initially, simulated smoke will want to rise because the particles and gases exceed ambient temperature (i.e., buoyancy-driven flow). Shortly after release, the simulated smoke will cool to the ambient temperature and it will then be transported due to natural convection or settling. One supplier stated that the simulated smoke temperature is less than 60°C, just inches from the nozzle, as required for safety. The flow of real smoke is buoyancy-driven due to the elevated temperature of the smoke (much greater than 60°C) emitted from the burning materials.

For all smoke generators, the liquid used to produce simulated smoke is pumped into a heat exchanger where it is vaporized, but the release of the simulated smoke from the heat exchanger can vary, as reported by several manufacturers. Some suppliers have stated that the smoke is released due to the vaporization pressure in the machine as well as pressure produced by the pump. Other machines use a propellant, such as CO_2 or N_2, to expel the smoke. The use of a pressurized gas will likely result in momentum-driven transport of the smoke instead of buoyancy-driven transport. In addition, the angle and method of release of the plume of

simulated smoke is very important to its transport. If the simulated smoke is released vertically, it will collect near the ceiling until the particles begin to settle. Smoke released at the floor could remain around the level it was released unless the smoke generator adds heat or a carrier gas, such as helium, to introduce buoyancy [1]. A patent exists on a smoke generator modified to include a helium carrier gas for the purpose of creating a buoyant plume [7].

The wide variety of available smoke generators will produce smoke with different morphological and transport properties; therefore, it will become necessary to consider which types of smoke generators produce a type and amount of simulated smoke that is comparable to actual smoke.

5. OPTICAL PROPERTIES.

Based on the morphology and composition of the smoke, the optical properties can be calculated. The extinction properties of the smoke are responsible for reducing visibility, and they are ultimately responsible for triggering the smoke detector alarm. The total extinction consists of two components: the portion of the light being absorbed and the portion of the light being scattered

$$\sigma_{ext} = \sigma_{abs} + \sigma_{scat} \tag{7}$$

In the following section, the mass-specific extinction (m^2/gm) will be calculated for actual and simulated smoke. Knowledge of the mass-specific extinction (σ_{ext}) can be used to calculate soot concentration based upon light extinction measurement, presently being performed at the FAA full-scale test facility. The light extinction measurements are based upon Bouguer's Law, which relates the light extinction coefficient (K in 1/m) and path length (L in m) to the ratio of the transmitted light (I/I_o) [8 and 9]

$$\frac{I}{I_o} = e^{-KL} = e^{-K_e \frac{f_v}{\lambda} L} = e^{-\sigma_{ext} M_s L} \tag{8}$$

where f_v is the volume fraction of soot, and λ is the wavelength of incident light.

The relation of the mass-specific extinction coefficient (σ_{ext}) to the light extinction coefficient (K in 1/m) and the dimensionless extinction coefficient (K_e) is

$$\sigma_{ext} = \frac{K}{M_s} = \frac{K_e f_v}{M_s \lambda} = \frac{K_e}{\rho_{soot} \lambda} \tag{9}$$

where M_s is the mass concentration of smoke (in kg/m^3).

The following section will characterize the extinction properties, (scattering and absorption) based on the morphology of actual and simulated smoke. The theory used to calculate the extinction properties is dependent on the size parameter, x, which is based on the size of the particle, D_p, and the wavelength, λ. The size parameter is defined as [10]

$$x = \frac{\pi D_p}{\lambda} \tag{10}$$

Considering a common visible laser wavelength (635 nm), the size parameter for actual soot is 0.39 (using D_p = 80 nm) and for simulated smoke it is 1.48 (D_p = 300 nm).

For $x << 1$, the particles are within the Rayleigh regime where scattering is assumed to be negligible. Typically, it is assumed that soot falls within the Rayleigh regime, although aggregation of the primaries typically causes this assumption to result in underestimation of the extinction by approximately 30% [4 and 11]. For $x = O(1)$, the extinction properties of the particles can be described by the complex Mie theory [10]. Simulated smoke droplets are in this range; therefore, Mie theory will be used to characterize the optical properties. For $x>>1$, the extinction properties are calculated using geometric optics where the surface of the particle is treated as a normal surface.

Actual soot does not fit into any of these three catagories very well. As stated before, aggregated soot particles are not likely within the Rayleigh regime. There have been attempts to find the optical properties of soot using the Mie theory by concentrating the entire mass of the soot agglomerate into an equivalent sphere, but this is not a good representation of a wispy chain [12]. Since soot is a fractal aggregate, the Rayleigh-Debye-Gans theory for polydisperse fractal aggregates (RDG-PFA) will be used to calculate the scattering and absorption properties for soot. Using the appropriate theory, the calculated optical properties for both actual and simulated smoke could provide insight into the effect of smoke type on detector certification.

5.1 ACTUAL SMOKE.

RDG-PFA can be used to calculate the scattering and absorption properties for soot. In using this theory, several assumptions about the properties of the soot are invoked, i.e., the soot consists of fractal aggregates, which obey the power law relation between number of primaries and radius of gyration (see equation 3); soot consists of spherical primary particles that just touch each other; and the index of refraction is uniform [4]. All of these appear to be valid as shown in figure 9.

Equations 11 through 13 for the mass-specific coefficients were derived from the total scattering and absorption cross sections [12]. The resulting equations were compared to the same derivation performed in a later paper [13], where it was determined that a typographical error existed. The sign of the exponent in the scattering term in the following equations has been corrected (positive value). The following equations display the derived expressions for the absorption and scattering properties of the soot as a function of their morphology.

$$\sigma_{abs} = \frac{6\pi E(m)}{\lambda \rho_p} \tag{11}$$

$$\sigma_{scat} = \frac{4\pi x_p^3 k_f F(m)}{\lambda \rho_p}\left(\frac{3D_f}{16x_p^2}\right)^{\frac{D_f}{2}} \tag{12}$$

$$\sigma_{ext} = \sigma_{abs} + \sigma_{scat} \tag{13}$$

where *E(m)* and *F(m)* are functions of the complex index of refraction of the soot. The complex index of refraction is defined as $m = n\text{-}ik$, where, n, is the ratio of the speed of electromagnetic radiation in a vacuum to the speed in the medium. For absorbing media (such as soot), the index of refraction is always complex and the k component is an indication of the absorptive property of the medium. The complex index of refraction for soot that will be used in all subsequent calculations is the one most frequently used, $m=1.57\text{-}i0.56$ [14]. Refractive indices of soot have been shown to be relatively independent of fuel type; therefore, the same refractive index will be used for all three fuel sources [15]. Note that simulated smoke is not an absorbing medium; therefore, its index of refraction will not contain an imaginary component (k). The functions, E and F, of the complex index of refraction used in calculating the extinction are

$$E(m) = Im\left(\frac{m^2 - 1}{m^2 + 2}\right) \tag{14}$$

$$F(m) = \left|\frac{m^2 - 1}{m^2 + 2}\right|^2. \tag{15}$$

The above equations for *E(m)* and *F(m)* can be used for $x \leq 0.1$, but for shorter wavelengths or larger particles (up to $x \approx 0.5$) *E(m)* should be replaced by *E'(m)*, defined in references 10 and 13 as

$$E'(m) = E(m) + \mathrm{Im}\left[\frac{x_p^2}{15}\left(\frac{m^2 - 1}{m^2 + 2}\right)^2\left(\frac{m^4 + 27m^2 + 38}{2m^2 + 3}\right)\right]. \tag{16}$$

Equations 11 through 16 were used to calculate the optical properties (extinction, scattering, and absorption) for all three types of actual smoke using the RDG-PFA theory, which has been shown to agree with measured properties within experimental uncertainty [15].

The RDG-PFA theory described above allowed for calculation of the extinction properties, including the relative contributions of scattering and absorption (shown in figures 17-19), which is not possible with typical cone calorimeter measurements. The scattering (thus extinction also) of the resin cake is slightly higher than the other two sources due to having both a larger primary particle size and fractal dimension. For all samples, the extinction (scattering and absorption) decreases as the wavelength of light increases for a constant particle size (from approximately 9 to 3 m^2/gm). From this analysis, it is evident that up to 30% of the total extinction can be attributed to scattering for actual soot from these three fire sources. This further validates the claim that treating soot particles to be in the Rayleigh regime results in a large error in the total extinction and other measurements drawn from the total extinction such as volume fraction (f_v). Overall, there is a good agreement in optical properties for the three different sources.

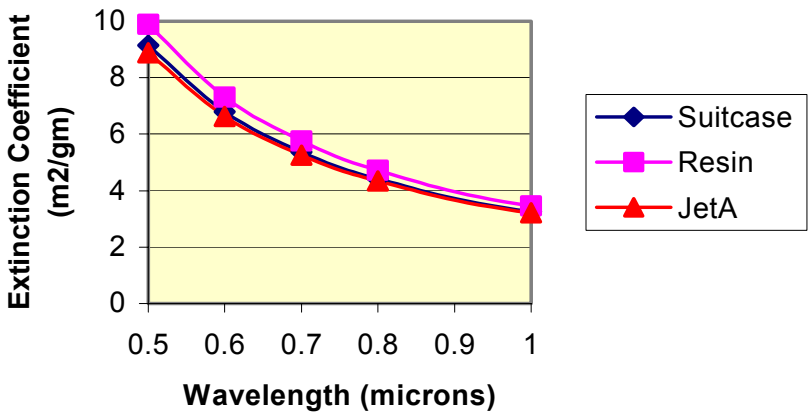

FIGURE 17. MASS-SPECIFIC EXTINCTION

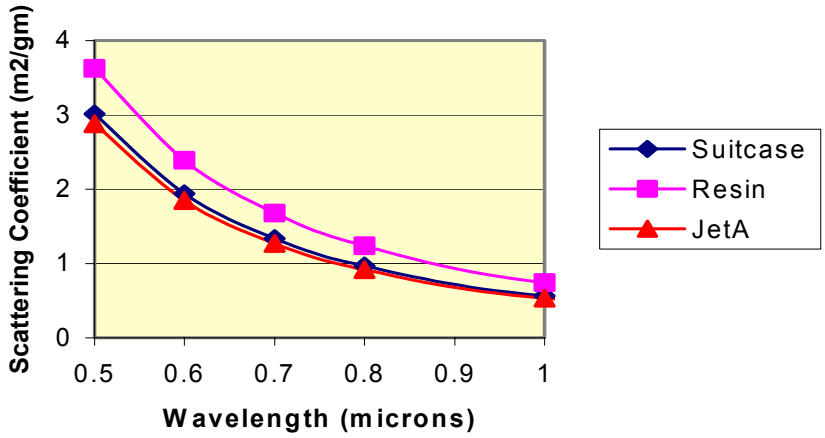

FIGURE 18. MASS-SPECIFIC SCATTERING

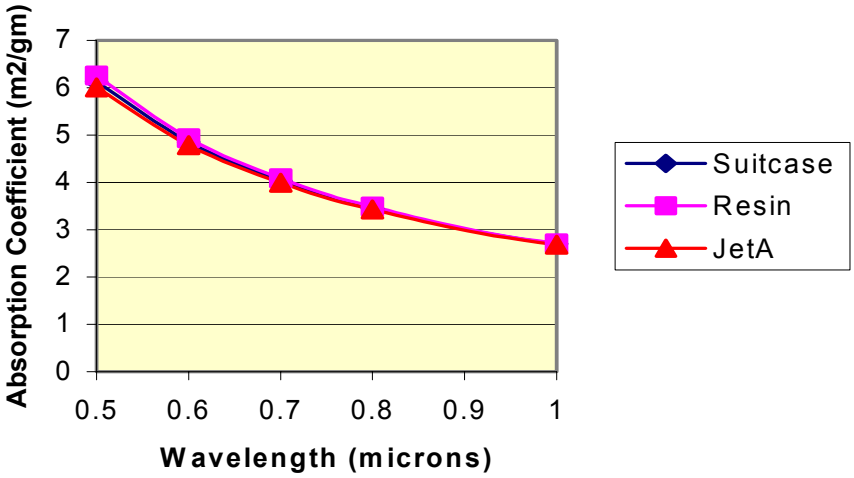

FIGURE 19. MASS-SPECIFIC ABSORPTION

Calculation of these properties proves useful in obtaining concentration (i.e., volume fraction or mass concentration) from light extinction measurements already being performed at the FAA full-scale test facility by using the extinction coefficient value corresponding to the wavelength of the lasers being used (see equation 17). Calculation of the soot volume fraction, using the specific extinction coefficient calculated in equations 11 through 13 using the RDG-PFA theory, should provide reliable results. The volume fraction of soot (f_v) can be calculated in the following manner: using K from the light extinction measurement, the value of σ_{ext} is calculated using the RDG-PFA theory and the density of the soot (ρ_{soot} in kg/m^3) [11 and 16]

$$f_v = \frac{K}{\sigma_{ext}\rho_{soot}} \tag{17}$$

5.2 SIMULATED SMOKE.

As stated previously, calculation of the size parameter allows one to assess the validity of the Mie theory for a particular size droplet and wavelength. Recall that for x=O(1), the extinction properties of the particles can be described by the complex Mie theory [10]. Simulated smoke droplets are in this range; therefore, the Mie theory will be used to characterize the optical properties.

A Mie theory computer code, based on the code in appendix A of reference 10, was used to calculate the optical properties of the simulated smoke. Two different sized simulated smoke droplets were considered: a 0.3-micron-diameter droplet corresponding to the average droplet size from the smoke generator study using supplier 1 (in table 3) and 0.66-micron droplets corresponding to the average droplet size obtained during a study performed at the FAA for a different smoke generator. These droplet sizes correspond to size parameters (x) from 0.94 to 4.1 for wavelengths less than 1 micron. The index of refraction used in the calculations was m = 1.4 (based on values of glycerol assumed to be very close to mineral oil or paraffin).

The optical properties for the two droplet sizes are shown in figures 20 and 21. Based on the plots, it is evident that all the extinction is due to scattering. The droplets do not have any absorptive capability, also indicated by the absence of the imaginary component of the refractive index. For the smaller droplets (0.3 micron), the extinction is a maximum of 5 m^2/gm for the smallest wavelength of 500 nm. The extinction decreases as the wavelength increases to a value below 1 m^2/gm for a wavelength of 1000 nm. For all wavelengths, the total extinction for the simulated smoke with this size droplet is approximately half of the extinction for actual smoke.

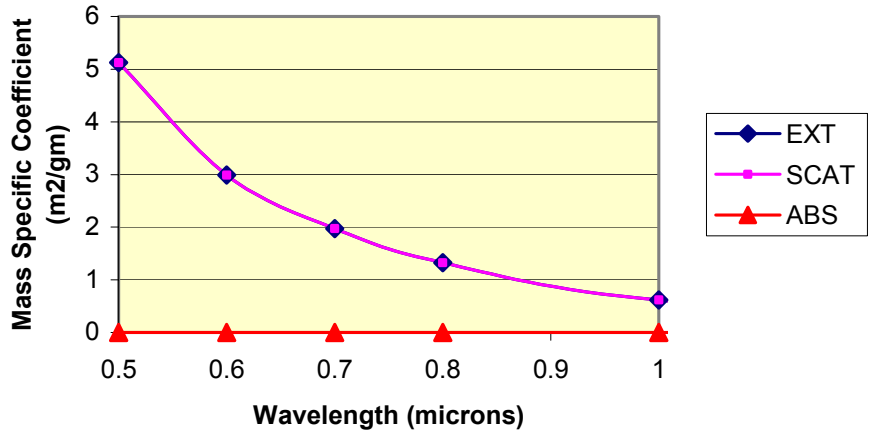

FIGURE 20. MASS-SPECIFIC COEFFICIENT FOR SIMULATED SMOKE (0.3 micron)

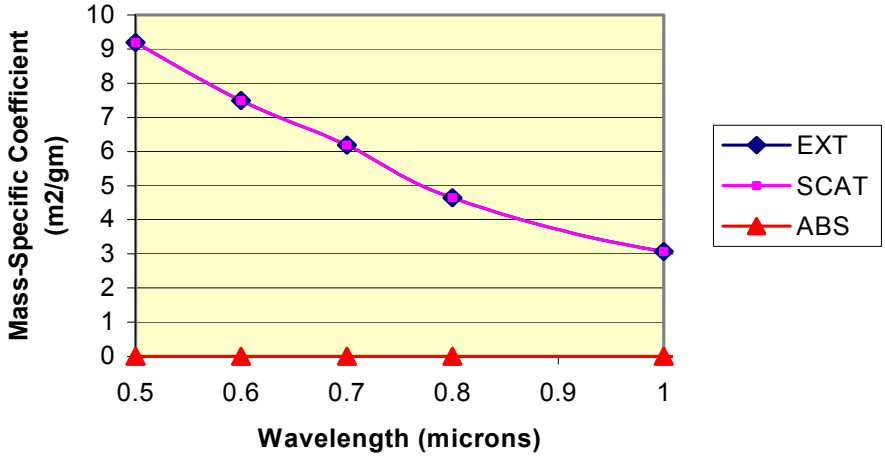

FIGURE 21. MASS-SPECIFIC COEFFICIENT FOR SIMULATED SMOKE (0.66 micron)

For the larger droplets (0.66 micron), the extinction is a maximum of 9 m^2/gm for the smallest wavelength of 500 nm. The extinction decreases as the wavelength increases to a value below 3 m^2/gm for a wavelength of 1000 nm. For all wavelengths, the total extinction for the simulated smoke with this size droplet is approximately equal to the extinction for actual smoke, although the scattering is significantly higher than the scattering for actual smoke.

A wide range of optical properties can exist for simulated smoke due to the range in droplet size produced by the generator. Even a single smoke generator can produce different sized droplets, depending on the machine setting. It has been shown that for the two different droplet sizes, all of the extinction is due to scattering for the simulated smoke, while only 30% of the extinction is due to scattering for the actual smokes.

5.3 APPLICATION TO DETECTION.

Current regulations require that cargo compartments be equipped with smoke detection systems that provide a visible indication of a fire. The detection systems should alarm within 1 minute of the start of the fire and before the fire has compromised the structural integrity of the aircraft [1]. Two different types of smoke detectors are readily available for use in a variety of applications. These two detectors, photoelectric and ionization, alarm when the output of a sensor changes in the presence of smoke. These detectors can also alarm due to nonfire sources such as dust, simulated smoke, and water vapor.

Photoelectric detectors contain a light source and a sensor (see figure 22). Under normal conditions, the light travels unimpeded across the chamber. If smoke is present in the chamber, light is scattered and some light is detected by the sensor. The detection of light by the sensor causes the device to alarm. Ionization detectors contain a small radiation source that ionizes the oxygen and nitrogen atoms in the air. The ionization (removal of an electron from the atom) creates a current due to the flow of positive and negative ions between two electrodes. When smoke enters the system it scavenges the ions, reduces the current, and produces an alarm. With knowledge of the operation of smoke detectors, the impact of the characteristics (morphology, transport, and optical properties) of actual and simulated smoke on detection times could be hypothesized.

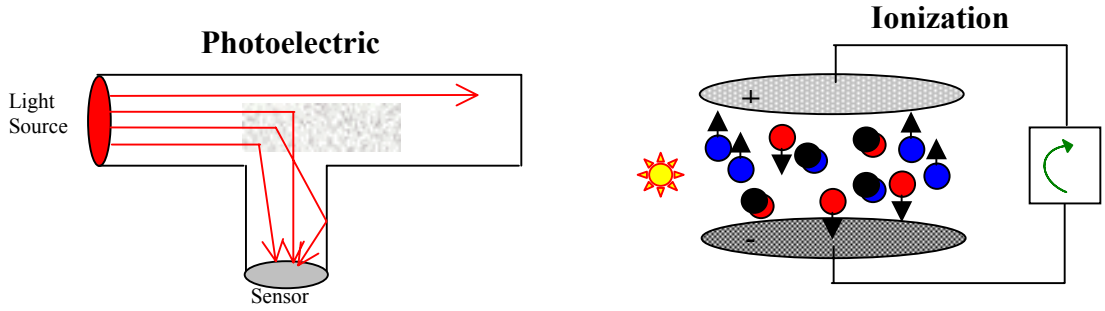

FIGURE 22. SCHEMATICS OF SMOKE DETECTORS

Photoelectric-type detectors are most commonly used in aircraft cargo compartments. As described above, these detectors alarm based on light scattered from smoke; therefore, the portion of the extinction due to scattering would have the most impact on smoke detection. The scattering properties of both simulated and actual smoke were calculated in the sections 5.1 and 5.2. All the extinction from simulated smoke is due to scattering, while only 20%-30% of the extinction is due to scattering for actual smoke. The mass-specific scattering is shown in figure 23 for all the smoke at visible wavelengths, since the source for most photoelectric detectors emits in the visible regime (some smoke detectors use an infrared light emitting diode as the light source). For both sizes of simulated smoke droplets, the scattering is greater than that calculated for any of the actual smokes. The scattering properties of the smaller simulated smoke droplets (0.3 micron) are similar to the actual smoke, although at short wavelengths the difference is fairly significant (up to 40%). The larger simulated smoke droplets (0.66 micron) scatter significantly more than any of the actual smoke. This considerable difference in scattering properties could result in significantly different detection times.

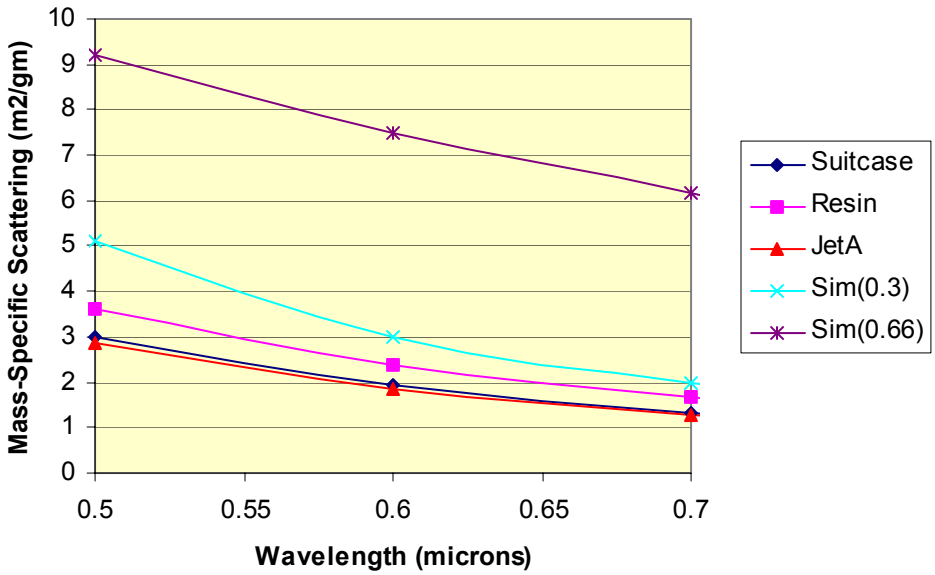

FIGURE 23. COMPARISON OF SCATTERING PROPERTIES

Properties of the smoke most likely to affect the alarm potential of the ionization detector are particle size, concentration, and transport. It is also believed that the particle charge (possibly also dependent on the composition) could likely play a role in the sensitivity of ionization detectors. Actual and simulated smoke are quite different with regard to morphology and composition; therefore, one could expect a different detector response, depending on the type of smoke.

6. SUMMARY OF RESULTS AND CONCLUSION.

This research provided insight into the morphology, transport, and optical properties of actual and simulated smoke. The following observations were made.

6.1 MORPHOLOGY.

- Soot from flaming fires (resin, suitcase and Jet A) was quantitatively characterized using thermophoretic sampling and subsequent analysis.
- Soot from smoldering fires was not characterized via transmission electron microscopy since the smoke did not contain solid particulate.
- Smoke from flaming fires was black, while smoke from smoldering fires was white (yellow on filter paper).
- Soot from all flaming fire sources consisted of spherical primary particles aggregated into wispy chains.

- The average primary particle diameter was 80 nm. The overall range of sizes within all samples was between 40 and 140 nm.
- The fractal dimension measurements (1.56-1.71) were consistent with visual observations and with values quoted in the literature.
- The fractal prefactor measurements (7.15-7.59) were consistent with values quoted in the literature.
- Overall, morphology of soot from all flaming sources was similar.

- Simulated smoke consists of droplets created when heated liquid condenses upon being expelled from the generator.
- Characterization of the morphology was obtained from the machine manufacturer.
- The droplet sizes for simulated smoke varied greatly (0.2-60 microns). Even a single machine could be operated under various conditions producing simulated smoke with very different morphological properties.
- The morphology of simulated smoke is considerably different from actual smoke because
  - actual smoke consists of solid particulate while simulated smoke is a fog (i.e., droplets).
  - the size of the individual primaries in actual smoke are a minimum of 3 times smaller than the simulated smoke droplets.
  - actual smoke primaries agglomerate into chains.
  - great variation was found in simulated smokes (even from a single machine), while actual smoke appear to have a relatively narrow range of characteristics for different fires and fuels.

6.2 TRANSPORT.

- Transport of actual and simulated smoke was analyzed with knowledge of morphology and density.
- Based on the results from the force balance equations, simulated smoke droplets are small enough to be transported with the flow. Actual smoke particulate will also follow the flow.
- The driving potential for transport could differ between actual fire sources and simulated smoke sources. Smoke from actual fires is buoyancy-driven due to the increased temperature, while simulated smoke transport may be momentum-driven due to the lower temperatures and forced expulsion from the vaporization chamber.

- A smoke generator modified with helium could provide buoyancy, therefore making the transport more like actual smoke.

6.3 OPTICAL PROPERTIES.

- With knowledge of the morphology and composition, the optical properties of actual and simulated smoke were calculated.

- The RDG-PFA theory was used to calculate the optical properties of actual soot since agglomerated soot are not within the Rayleigh regime, and the Mie theory for an equivalent sphere has typically been inadequate.

- For actual smoke, the total extinction decreased as the wavelength increases (from a maximum of 10 m^2/gm at 500 nm to 3 m^2/gm at 1000 nm).

- The scattering accounted for 30% of the total extinction for actual smoke.

- The overall extinction of all three actual smokes was very similar and also agreed with the range typically stated in the literature. The scattering from the resin cake was slightly higher due to the larger primaries and fractal dimension.

- For simulated smoke, the total extinction decreased as the wavelength increased and the total extinction was greater for the bigger droplets (0.66 micron).

- All the extinction was due to scattering for the simulated smoke.

- The extinction for the smaller droplets (0.3 micron) was approximately half of the total extinction for the actual smokes from 0.5-1 micron wavelengths, while the extinction for the larger droplets was approximately the same as the actual smokes.

- The scattering for the smaller droplets was slightly higher than the actual smoke, but the scattering for the larger droplets was almost double the actual smoke scattering. This could have a great impact on detection time for photoelectric smoke detectors.

- Knowledge of optical properties can be used to calculate soot volume fraction from extinction measurements in the full-scale model validation experiments.

As summarized above, this research characterized the dominant features of actual and simulated smoke used in the certification of aircraft cargo compartment detection systems. The smoke from actual flaming fires and aerosol generators was compared based upon morphological, optical, and transport properties. Several differences were noted that will likely impact the way detection systems interact with simulated smoke compared to actual smoke. Minimization of this affect could be acheived through careful selection and standardization of simulated smoke sources.

6.4 CONCLUSION.

Standardization of the in-flight certification process through characterization of simulated smoke generators (specification of machine, operating setting, etc.) is the only way to ensure all cargo compartment detection systems are being certified under similar conditions. Calculation of the extinction, scattering, and absorption for the characterized simulated smoke could be performed using the Mie theory code. Comparison with the results from the actual smoke characterization using the RDG-PFA theory could ensure that a suitable simulated smoke source is being used that should interact with the detector in the same way as the intended actual fire source.

7. REFERENCES.

1. Advisory Circular, AC 25-9A, "Smoke Detection, Penetration, and Evacuation Tests and Related Flight Manual Emergency Procedures," 1994.

2. Williams, J.M. and Gritzo, L.A., "In-Situ Sampling and Transmission Electron Microscope Analysis of Soot in the Flame Zone of Large Pool Fires," *27th International Symposium on Combustion*, 1998.

3. R.A. Filipczak, D. Blake, L. Speitel, R.E. Lyon, J.M. Suo-Anttila, and W. Gill, "Development and Testing of a Plastic Smoke Generation Source," *Proceedings of the Fire and Materials Conference*, January 2001.

4. Köylü and Faeth, *Combustion Science and Technology*, 108:207-229 (1995a).

5. Krishnan, S.S., Lin, K.C., Faeth, G.M., *Journal of Heat Transfer*, 2001; **123**: 331.

6. Haynes, B.S., Wagner, H.G.G., *Progress in Energy and Combustion Science*, 1981; **7**: 229.

7. Eklund, T.I., "Generation of a Buoyant Plume of Artificial Smoke for Airplane Tests," DOT/FAA/CT-90/9, September 1990.

8. "The SFPE Handbook of Fire Protection Engineering" (1995).

9. Dobbins, R.A. and Megaridis, C.M., "Absorption and Scattering of Light by Polydisperse Aggregates" *Applied Optics*, Vol. 30, No. 33, 1991.

10. Bohren, C.F. and Huffman, D.R., "Absorption and Scattering of Light by Small Particles," 1983.

11. Choi, M.Y., Mullholland, G.W., Hamins, A., and Kashiwagi, T., "Comparisons of the Soot Volume Fraction Using Gravimetric and Light Extinction Techniques," *Combustion and Flame*, 102:161-169, 1995.

12. Köylü, U.O. and Faeth, G.M., "Radiative Properties of Flame Generated Soot," *Journal of Heat Transfer*, 115:409-417, 1993.

13. Dobbins, R.A., Mullholland, G.W., and Bryner, N.P., "Comparison of a Fractal Smoke Optics Model With Light Extinction Measurements," *Atmospheric Environment*, 28:889-897, 1994.

14. Smyth and Shaddix, "The Elusive History of m=1.57-0.56i for the Refractive Index of Soot," Brief Communication, *Combustion and Flame*, 107:314-320, 1996.

15. Wu, J.S., Krishnan, S.S., and Faeth, G.M., "Refractive Indices at Visible Wavelengths of Soot Emitted From Buoyant Turbulent Diffusion Flames," *Journal of Heat Transfer*, Vol. 119, May 1997.

16. Zhu, J., Choi, M.Y., Mullholland, G.W., and Gritzo, L.A., " Measurement of Soot Optical Properties in the Near-Infrared Spectrum," *International Journal of Heat and Mass Transfer*, 43: 3299-3303, 2000.